Unsteady Crack Motion and Branching in a Phase-Field Model of Brittle Fracture

Alain Karma and Alexander E. Lobkovsky
Department of Physics and Center for Interdisciplinary Research on Complex Systems, Northeastern University, Boston, Massachusetts 02115, USA
(Received 7 January 2004; published 18 June 2004)

Crack propagation is studied numerically using a continuum phase-field approach to mode III brittle fracture. The results shed light on the physics that controls the speed of accelerating cracks and the characteristic branching instability at a fraction of the wave speed.

DOI: 10.1103/PhysRevLett.92.245510 PACS numbers: 62.20.Mk, 46.50.+a, 46.15.–x

The quest for a fundamental understanding of dynamic brittle fracture has been an ongoing challenge. The traditional continuum theory of brittle fracture consists of solving the equations of linear elasticity with boundary conditions on the moving fracture surfaces up to the crack tip [1]. The solutions have stress fields that diverge near the tip, representing a finite energy flow rate to the tip. The crack propagation speed v is assumed to be uniquely determined by this energy flow rate. All the nonlinear physics of failure inside a microscopic region around the tip—the so-called process zone—is buried in a phenomenological function that relates the fracture energy Γ of the material (energy to advance the tip per unit length of crack front and per unit of crack extension) and v.

The main difficulty in any experimental test of this theory is that the energy flux to the tip cannot be measured directly but needs to be inferred from a time-dependent solution of linear elasticity for accelerating cracks. Using an approximate solution, Sharon and Fineberg found that a unique $\Gamma(v)$ curve describes cracks accelerated under different loads, thereby validating the continuum theory [2]. Kessler and Levine obtained the same result in lattice simulations [3] using an exact solution of Eshelby [4] for accelerating cracks. These authors, however, found that the experimental data of Ref. [2] do not collapse on a single $\Gamma(v)$ curve when interpreted using Eshelby's solution.

Also of long-standing interest is a generic dynamic instability that limits the speed of fast moving cracks in both experiments [2,5,6] and molecular dynamic simulations [7]. The fact that microscopically very different amorphous materials [such as glass and poly(methyl methacrylate)] exhibit strikingly similar branching instabilities [2] strongly suggests that a continuum theory may be appropriate for understanding this phenomenon. Devising such a theory, however, has proven to be difficult. Cohesive zone theories modify the boundary conditions on the stress field near the tip to take into account the short-scale force between crack surfaces. Langer and Lobkovsky [8], however, have shown that these models are unsuitable for stability calculations since the results depend singularly on the details of the cohesive zone. In addition, intrinsically discrete branching instabilities in lattice models [9,10] seem unlikely to bear relevance to experiments in amorphous materials.

In this Letter, we study dynamic brittle fracture using a recently developed continuum phase-field approach for mode III cracks [11]. This approach has the chief advantage that it incorporates both the short-scale physics of failure and the macroscopic linear elasticity within a self-consistent set of coupled nonlinear partial differential equations that can be solved numerically. An earlier study of this model did not show a branching instability because the simulations were restricted to very small systems, not much larger than the process zone size [11]. Here, we overcome the intrinsic stiffness of the phase-field equations, which allows us to carry out simulations in system sizes an order of magnitude larger. These simulations reveal that the characteristic branching instability at a fraction of the wave speed is a robust feature of the phase-field model. In addition, we obtain system-size independent results that can be meaningfully compared to results from the fracture community.

The basic variables of the model [11] are the scalar displacement $u(x, y)$ perpendicular to the x-y plane of mass points from their original positions, and the phase field, $\phi(x, y)$, which describes the state of the material. The unbroken solid, which behaves purely elastically, corresponds to $\phi = 1$, whereas the fully broken material that cannot support stress corresponds to $\phi = 0$. The total energy (kinetic plus elastic) of the system per unit length of the crack front is

$$E = \int dxdy \Big[\frac{\rho}{2}(\partial_t u)^2 + \frac{\kappa}{2}|\vec{\nabla}\phi|^2 + hf(\phi) + \frac{\mu}{2} g(\phi)(|\vec{\epsilon}|^2 - \epsilon_c^2) \Big], \quad (1)$$

where ρ is the density, $\vec{\epsilon} \equiv \vec{\nabla} u$ is the strain, $f(\phi)$ is a double-well potential with minima at $\phi = 1$ and $\phi = 0$, μ is the elastic shear modulus, and ϵ_c is the critical strain magnitude such that the unbroken (broken) state is energetically favored for $|\vec{\epsilon}| < \epsilon_c$ ($|\vec{\epsilon}| > \epsilon_c$). The function $g(\phi)$ is a monotonously increasing function of ϕ with limits $g(0) = 0$ and $g(1) = 1$, which controls the softening of the elastic energy at large strain.

Taking the first variations of the energy with respect to the strain and to ϕ, we obtain the stress, $\vec{\sigma} = \delta E/\delta\vec{\epsilon}$, and the equations of motion,

$$\chi^{-1}\partial_t\phi = -\frac{\delta E}{\delta\phi} = \kappa\nabla^2\phi - hf'(\phi) - \mu g'(\phi)(|\vec{\nabla}u|^2 - \epsilon_c^2), \tag{2a}$$

$$\rho\partial_t^2 u = \vec{\nabla}\cdot\vec{\sigma} = \mu\vec{\nabla}\cdot[g(\phi)\vec{\nabla}u], \tag{2b}$$

where $f' \equiv df/d\phi$ and $g' \equiv df/d\phi$. Energy is dissipated in the process zone around the crack tip where ϕ varies rapidly in space and time. Equation (2a) implies that the size of the process zone is $\xi = \sqrt{\kappa/\mu\epsilon_c^2}$, and the characteristic time of energy dissipation in this zone is $\tau = 1/(\chi\mu\epsilon_c^2)$. Furthermore, by rescaling lengths by ξ, time by ξ/c, where $c \equiv \sqrt{\mu/\rho}$ is the shear wave speed, and u by $\xi\epsilon_c$, we find that the crack propagation in Eqs. (2) is controlled by only two dimensionless parameters: $\delta = h/(\mu\epsilon_c^2)$ and $\beta = c\tau/\xi$. The first determines the dimensionless surface energy [11] $\tilde{\gamma} \equiv \gamma/(\mu\epsilon_c^2\xi) = \int_0^1 d\phi[1 - g(\phi) + 2\delta f(\phi)]^{1/2}$, which is order unity for $\delta = 0$. With $f(\phi) = 16\phi^2(1-\phi)^2$ and $g(\phi) = 4\phi^3 - 3\phi^4$, $\tilde{\gamma}$ approximately doubles when δ increases from 0 to 2. The second parameter β controls the importance of inertia relative to dissipation in the process zone. If $\tau \gg \xi/c (\beta \gg 1)$, then bond breaking is sluggish and the displacement field relaxes rapidly to a quasistatic configuration around the process zone. Therefore, the crack propagation speed is limited by the rate of dissipation in the process zone. In the opposite limit $\tau \ll \xi/c (\beta \ll 1)$, bond breaking is quasi-instantaneous and the rate of crack propagation is limited by the inertial dynamics of the displacement field. The total energy is in fact conserved in the extreme inertia-dominated limit $\beta \to 0$ [see Eq. (4) below] where dissipation plays no role.

We study fracture numerically in a strip of width $2W$ with a fixed displacement $u(x, \pm W) = \pm\Delta$ at the strip edges. The stored elastic energy per unit area ahead of the crack tip is $G = \mu\Delta^2/W$, and the Griffith's threshold load for a semi-infinite crack is $G_c = 2\gamma$. The phase-field equations are made extremely stiff by the localization of strain within a narrow region whose width vanishes in the large strip limit $W/\xi \to \infty$ [11]. To overcome this stiffness, we discretize the energy density on a square lattice:

$$\frac{E}{a^2} \approx \sum_{i,j}\frac{\rho}{2}(\partial_t u_{ij})^2 + \frac{\kappa}{2a^2}[(\phi_{i+1j} - \phi_{ij})^2 + (\phi_{ij+1} - \phi_{ij})^2] + hf_{ij} + \frac{\mu}{2}\left(\frac{g_{ij} + g_{i+1j}}{2a^2}(u_{i+1j} - u_{ij})^2 + \frac{g_{ij+1} + g_{ij}}{2a^2}(u_{ij+1} - u_{ij})^2 - g_{ij}\epsilon_c^2\right), \tag{3}$$

where the subscripts i and j refer to position $(x = ia, y = ja)$ on the lattice and we have defined $f_{ij} \equiv f(\phi_{ij})$ and $g_{ij} \equiv g(\phi_{ij})$. Next, we obtain the equations of motion variationally from this energy, $a^2\chi^{-1}\partial_t\phi_{ij} = -\partial E/\partial\phi_{ij}$ and $a^2\rho\partial_t^2 u_{ij} = -\mu\partial E/\partial u_{ij}$, which reduce to Eqs. (2a) and (2b), respectively, in the continuum limit $a \to 0$. This approach has the chief advantage that the lattice spacing needs only to be chosen small enough to resolve the smooth spatial variation of the two coupled fields ϕ and u in the process zone. The discontinuity of the displacement field on the lattice scale behind the crack tip does not influence the crack dynamics, except through multiple reflections of high-frequency waves at large time. This radiation is easily suppressed by damping waves at boundaries or adding a small Kelvin viscosity to Eq. (2b), with no qualitative change of the results presented here. We have verified that the important observables converge quickly in the limit of the vanishing lattice spacing and that we operate in the regime where these observables differ by at most 15% from their continuum limits for a in the range 0.3 to 0.4ξ.

To study unsteady crack propagation as in previous experiments [2] and lattice simulations [3], we first compute stationary cracks of different initial lengths ℓ and loads G. These solutions are found by solving Eq. (2b) without inertia with a Gauss-Seidel iteration scheme and by relaxing ϕ using Eq. (2a). We then simulate the full equations of motion with inertia, with these solutions as initial conditions. To study steady-state features of crack propagation independent of initial conditions, we run long simulations in strips that are effectively infinite along the propagation direction. To keep the computations tractable, we periodically translate the fields u and ϕ by one lattice spacing such that the crack tip remains in the middle of a strip of length much larger than W. We have checked that the results of these "treadmill" simulations are independent of boundary effects.

To compute the fracture energy, we equate $v\Gamma$ with the expression for the energy flow rate to the tip of mode III cracks [4] $v\Gamma = \int_C dC[\mu\dot{u}\partial_n u + vn_x\partial_t(\rho\dot{u}^2/2 + \mu|\vec{\epsilon}|^2/2)]$, where C is a closed circuit around the moving tip and $\hat{n}$ is the outward normal to C. More precisely, we calculate the time rate of change of the total kinetic plus elastic energy in the region where ϕ is larger than a threshold value ϕ_c close to unity. This quantity is precisely the energy flow rate into the process zone defined as the region where $\phi < \phi_c$.

Plots of tip speed versus tip position for cracks accelerating from rest are shown in Fig. 1 for the inertia-dominated regime $\beta = 1$. Corresponding plots of Γ versus v are shown in Fig. 2. The initial crack acceleration increases with load, and the tip splits into two symmetric branches above a critical onset load G_{onset}. Cracks for smaller loads that do not split, or split only transiently for $G \sim G_{\text{onset}}$, reach a steady-state velocity equal to the steady-state velocity calculated on the treadmill (solid line in Fig. 2). The equality $\Gamma = G$ in steady state is a self-consistency check of our method of calculating Γ.

From the long simulations on the treadmill, three basic regimes of crack propagation can be distinguished: a stable steady-state regime for small loads, where v is

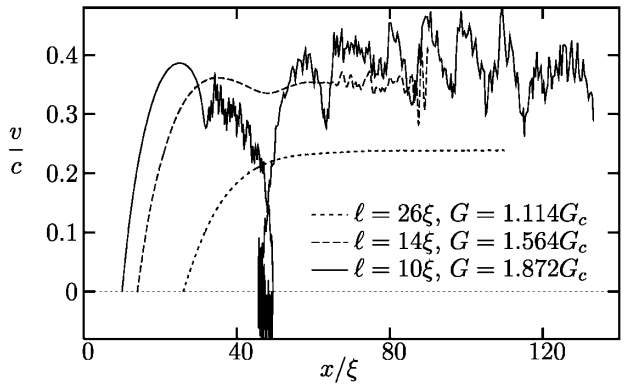

FIG. 1. Crack speed $\dot{x}(t)$ versus tip position $x(t)$ for accelerating cracks with different initial lengths, where $x(t)$ is the point of the $\phi = 1/2$ contour with the largest x. $\beta = 1$, $\delta = 0$, $a = 0.3\xi$, and $W = 30\xi$. The speed can become negative when branches retreat transiently.

constant in time and the crack is rectilinear; an asymmetric tip-splitting ("snake") mode for intermediate loads, where v fluctuates in time around some average value while the crack follows a sinusoidal trajectory; and a chaotic tip-splitting regime with well-developed branches for large loads. Examples of these regimes are shown in Fig. 3. The steady-state velocity v saturates at some value v_c. Rectilinear cracks cannot propagate faster than v_c. These results suggest that off-axis branching in the present model is due to the absence of steady-state crack solutions above a critical speed. The dependence of v_c on the parameters of the model is shown in Fig. 4. The maximum crack speed is well defined in the inertia-dominated limit $\beta \to 0$. It grows monotonically with the scaled surface energy $\tilde{\gamma}$ and has a minimum at $\delta = 0$ of $v_c \approx 0.41c$. At this speed, the linear elastic field in the unbroken material around the crack tip is quasi-isotropic [12]. We therefore conjecture, along the lines of Gao [13], that tip blunting, which leads to velocity saturation and ultimately to tip splitting, is due to the

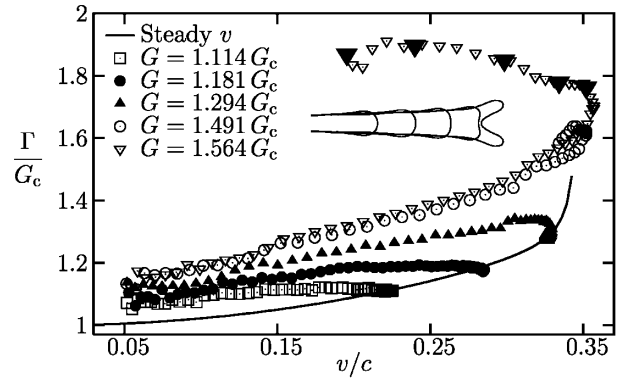

FIG. 2. Fracture energy versus tip speed for the accelerating cracks of Fig. 1. The solid line corresponds to steady-state propagation with $\Gamma = G$ by energy conservation. The $\phi = 1/2$ contours in the inset are spaced in time by $10\xi/c$ and correspond to the large solid triangles.

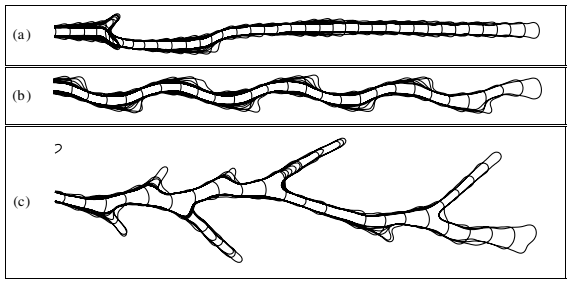

FIG. 3. Contours of $\phi = 1/2$ separated in time by $10\xi/c$. Plots are on the same scale for a strip width $W = 30\xi$, $\beta = 2$, and $\delta = 0$. (a) Transient branching for $G = 1.56G_c$. (b) Weak periodic branching (the snake) for $G = 1.86G_c$. (c) Chaotic branching for $G = 2.90G_c$.

relativistic contraction of stress fields in the nonlinear process zone where the sound speed is small due to the softening of the material.

Our results are in reasonably good agreement with the analytical calculation of Adda-Bedia [14], which predicts that tip splitting is energetically possible for mode III fracture for speeds above $0.39c$ with an angle between symmetric branches of 80°. For comparison, the smallest value of v_c is about $0.41c$ in the $\beta \to 0$ limit of the simulations. Furthermore, the branching angle is close to 70° near the onset of branching and decreases for larger loads, as shown in Fig. 5. It should be noted, however, that v_c depends on the surface energy $\tilde{\gamma}$ in the simulations, as shown in the inset of Fig. 4, whereas it is independent of the latter in the energetic calculation of Ref. [14], which only considers the energy flow to the tip within the framework of macroscopic linear elasticity. This difference shows that the cohesive forces on the scale of the process zone also influences branching.

It is important to emphasize that the limiting speed of crack propagation and the branching angle are both independent of system size in our simulations. In addition, well-developed branches follow a smooth curved path, as shown in the inset of Fig. 5 and as seen experimentally [2]. Interestingly, even though our simulations are for mode III and the experiments are for mode I, branch

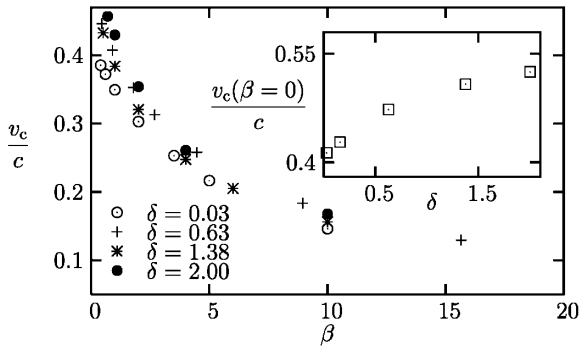

FIG. 4. Limiting speed of crack propagation v_c versus β for different values of δ. Inset: v_c in the inertia-dominated ($\beta \to 0$) limit versus δ.

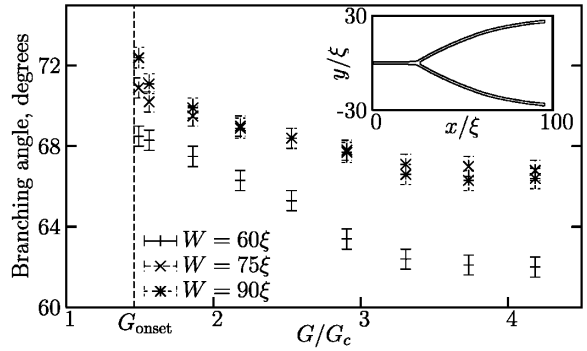

FIG. 5. Angle between symmetric branches as a function of load for cracks accelerated from rest in different strip widths. The inset shows an example of branching ($\phi = 1/2$ contour) for $W = 75\xi$. The results are independent of system size for the two largest strip widths.

shapes are well fit by a power law of the form $y \sim x^{\nu}$, with $\nu \approx 2/3$ in both experiments and simulations for $y \gg \xi$. The system size, however, can influence the dynamics at larger time after the onset of the instability through the coupling of the tip dynamics to reflected waves. One clear example is the snakelike oscillatory solution of Fig. 3(b) for $W = 30\xi$, where the tip oscillates with a period $4\ W/c$ close to the first harmonic standing wave in the strip. This oscillation is on the scale of the process zone and would not be observable experimentally. In contrast, for larger loads and strips widths, the mean spacing between well-developed branches in the chaotic branching regime appears to be more weakly dependent on system size.

To further interpret our results, let us first derive an analytic expression for the speed of steady-state cracks close to the Griffith threshold. Energy balance implies that the stored elastic energy ahead of the crack in excess of 2γ must be dissipated in the process zone, or

$$v(G - G_c) = -dE/dt = (1/\chi) \int dxdy(\partial\phi/\partial t)^2, \quad (4)$$

where the second equality follows from Eqs. (2) with no energy flux through the boundaries. In a coordinate system $(x' = x - vt,\ y' = y)$ translating with the tip, $\partial\phi/\partial t = -v\,\partial\phi/\partial x'$. Thus the steady-state velocity of rectilinear crack propagation is

$$v/c \approx 2\tilde{\gamma}(G/G_c - 1)/(\beta I), \quad (5)$$

where $I \equiv \int dx'dy'(\partial\phi/\partial x')^2$ is a dimensionless integral factor of order unity that depends on the profile of ϕ for a stationary crack at $G \approx G_c$. This prediction is consistent with the simulation results that show a steeper increase of velocity with a load for smaller β.

The fact that the $\Gamma - v$ plots for different accelerating cracks in Fig. 2 do not superimpose on the steady-state curve clearly shows that v is not uniquely determined by the energy flow rate to the tip. This cannot be explained by the modification of this energy flow rate due to wave reflections [15] since the lack of data collapse is already present for times shorter than the wave reflection time. In our model, accelerating cracks require more energy per unit length of advance than steadily propagating cracks. This extra energy is reversibly stored in the process zone to be either consumed by branching or radiated away later. This effect is exacerbated for large loads and causes the crack to decelerate before branching. This deceleration is marked by the overshoot of the velocity versus the tip position (Fig. 1), which has been observed for very large accelerations in brittle fracture of glass [2].

To estimate crudely the importance of acceleration, let us assume that its effect becomes negligible when the change of the crack speed over a distance $\sim\xi$ is small compared to the wave speed, or $\xi d(v/c)/dx \ll 1$. This inequality can also be written as $d(v/c)/d(G/G_C) \times \xi d(G/G_C)/dx \ll 1$. Equation (5) implies that $d(v/c)/d(G/G_C) \sim \tilde{\gamma}/\beta$, whereas $\xi d(G/G_C)/dx \sim \xi/W$. The fact that $\Gamma - v$ plots do not collapse on a single curve in simulations with β and G/G_c of order unity, and $W/\xi \approx 100$, shows that acceleration effects persist for much larger system sizes than this estimate predicts. This breakdown of the continuum theory of brittle fracture in the present model remains to be understood.

This study shows that the phase-field method is a promising approach to investigate instabilities in brittle fracture. The extension of this model to other modes of fracture and higher dimensions is in principle straightforward by modifying the energy functional [Eq. (1)]. A much harder task for the future, however, is the incorporation of more realistic mechanisms of failure in order to make quantitative predictions for specific materials.

This research is supported by U.S. DOE Grant No. DE-FG02-92ER45471.

[1] L. B. Freund, *Dynamic Fracture Mechanics* (Cambridge University Press, Cambridge, England, 1990).
[2] E. Sharon and J. Fineberg, Nature (London) **397**, 333 (1999).
[3] D. A. Kessler and H. Levine, Phys. Rev. E **68**, 036118 (2003).
[4] J. D. Eshelby, J. Mech. Phys. Solids **17**, 177 (1969).
[5] T. Cramer *et al.*, Z. Metallkd. **90**, 675 (1999); Phys. Rev. Lett. **85**, 788 (2000).
[6] K. Ravichandar and W. G. Knauss, Int. J. Fract. **25**, 247 (1984).
[7] F. F. Abraham *et al.*, Phys. Rev. Lett. **73**, 272 (1994); D. Holland and M. Marder, Phys. Rev. Lett. **80**, 746 (1997).
[8] J. S. Langer and A. E. Lobkovsky, J. Mech. Phys. Solids **46**, 1521 (1998).
[9] M. Marder and X. Liu, Phys. Rev. Lett. **71**, 2417 (1993).
[10] D. A. Kessler and H. Levine, Phys. Rev. E **63**, 016118 (2001).
[11] A. Karma *et al.*, Phys. Rev. Lett. **87**, 045501 (2001).
[12] E. H. Yoffe, Philos. Mag. **42**, 739 (1951).
[13] H.-J. Gao, J. Mech. Phys. Solids **44**, 1453 (1996).
[14] M. Adda-Bedia, J. Mech. Phys. Solids (to be published).
[15] M. Marder, Phys. Rev. Lett. **66**, 2484 (1991).